American Mineralogist, Volume 108, pages 439–446, 2023

Solid solution of $CaSiO_3$ and $MgSiO_3$ perovskites in the lower mantle: The role of ferrous iron

Feiwu Zhang[1,*,†], Tingting Xiao[1,2], and Joshua M.R. Muir[1,*,‡]

[1]State Key Laboratory of Ore Deposit Geochemistry, Institute of Geochemistry, Chinese Academy of Sciences, Guiyang 550081, China
[2]CAS Key Laboratory of Crust-Mantle Materials and Environments, School of Earth and Space Sciences, University of Science and Technology of China, Hefei 230026, China

Abstract

The solid solution between $CaSiO_3$ and $MgSiO_3$ perovskites is an important control on the properties of the lower mantle but the effect of one of the most important impurity elements (iron) on this solution is largely unknown. Using density functional theory (DFT), ferrous iron's influence on the reciprocal solubility of $MgSiO_3$ and $CaSiO_3$ perovskite (forming a single Ca-Mg mixed perovskite phase) was calculated under pressures and temperatures of 25–125 GPa and 0–3000 K, respectively. Except at iron-rich conditions, ferrous iron preferentially partitions into the mixed perovskite phase over bridgmanite. This is a small effect (partitioning coefficient K_D ~0.25–1), however, when compared to the partitioning of ferrous iron to ferropericlase, which rules out perovskite phase mixing as a mechanism for creating iron-rich regions in the mantle. Iron increases the miscibility of Ca and Mg perovskite phases and reduces the temperature at which the two perovskite phases mix but this effect is highly nonlinear. We find that for a pyrolytic mantle [Ca% = 12.5 where Ca% = Ca/(Ca+Mg)] a perovskite ferrous iron concentration of ~13% leads to the lowest mixing temperature and the highest miscibility. With this composition, 1% ferrous iron in a pyrolytic composition would lead to mixing at ~120 GPa along the geothermal gradient, and 6.25% ferrous iron leads to mixing at ~115 GPa and 13% ~110 GPa. At high iron concentrations, Fe starts to impair miscibility, with 25% ferrous iron leading to mixing at ~120 GPa. Thus, in normal pyrolytic mantle, iron could induce a small amount of Ca-pv and Mg-pv mixing near the D″ layer but it generally partitions to ferropericlase instead and does not impact mixing. Extremely iron rich parts of the lower mantle such as ULVZs or the CMB (potentially) are also not a likely source of phase mixed perovskites due to the nonlinear effect of ferrous iron on phase mixing.

Keywords: $CaSiO_3$, $MgSiO_3$, iron, miscibility, the lower mantle; Physics and Chemistry of Earth's Deep Mantle and Core

Introduction

Earth's lower mantle, extending from 660 to 2890 km in depth, occupies nearly 75% of the mass of the bulk silicate Earth. Assuming that the lower mantle is pyrolytic and isochemically similar to the upper mantle, $MgSiO_3$ perovskite (bridgmanite) is considered to be the most abundant phase in the lower mantle, accounting for about 70% of the lower mantle, followed by ferropericlase (about 20%), and finally the least abundant phase is $CaSiO_3$-rich perovskite (Davemaoite) accounting for around 6–12% (Anderson et al. 1989; O'Neill and Jeanloz 1990). Mg-rich silicate perovskite (Mg-pv) and $CaSiO_3$-rich perovskite (Ca-pv) are thus two of the main components of the lower mantle and subducted plates. Due to their similarity in chemical formula and structure, these two phases can dissolve into each other to some extent, forming a single $Mg_{1-x}Ca_xSiO_3$ phase. Mixing of these phases is potentially important as a chemically mixed Ca-Mg-pv phase will likely behave differently to a physical mixture of Ca-pv and Mg-pv. We are not aware of any studies of the physical properties of a Ca-Mg-pv phase but first it is important to establish whether this phase can exist in the mantle.

The solubility of Ca in Mg-pv and Mg in Ca-pv has been previously studied, and it is generally found that these two phases have very limited mutual solubility under lower mantle conditions (Armstrong et al. 2012; Fujino et al. 2004; Irifune et al. 1989, 2000; Jung and Schmidt 2011; Muir et al. 2021; Tamai and Yagi 1989; Vitos et al. 2006). This limited solubility is speculated to be due to the large size difference between Mg^{2+} and Ca^{2+}, which could reduce the miscibility (Jung and Schmidt 2011; Kesson et al. 1995; Vitos et al. 2006). As the lower mantle is more Mg rich than Ca rich, we shall focus on the solubility of Ca in Mg-pv. Experimentally Irifune et al. (1989) found that the solid solubility of Ca in Mg-pv was limited to 2% or even lower at 25 GPa and ~1800 K. Armstrong et al. (2012) found that at 2000 K, the solubility of Ca in Mg-pv is <5% at 30 GPa and at least 10% at 55 GPa. With increasing pressure, the solubility thus increases. Theoretically Jung and Schmidt (2011) found that the solubility of Ca in Mg-pv was 0.5% at 25 GPa and 2000 K, but 5% at 25 GPa and 3000 K, and Vitos et al. (2006) claimed that under the temperature and pressure conditions of the upper mantle and transition zone, the solid solubility of Ca in Mg-pv is 4–6%. Jung and Schmidt (2011) and Vitos et al. (2006) found that pressure decreased the solid solubility of Ca in Mg-pv in contrast with experimental findings (Armstrong et al.

* E-mail: zhangfeiwu@vip.gyig.ac.cn; j.m.r.muir@mail.gyig.ac.cn
† Orcid 0000-0002-4979-0790
‡ Special collection papers can be found online at http://www.minsocam.org/MSA/AmMin/special-collections.html.

0003-004X/23/0003–439$05.00/DOI: https://doi.org/10.2138/am-2022-8356

2012). This was rectified by our recent study (Muir et al. 2021) where we found that the explicit inclusion of vibrational entropy caused pressure to increase miscibility; the results demonstrated that above the D″ in the lower mantle, pyrolytic compositions of Mg-pv and Ca-pv will not mix. Thus, all previous studies agree that pure Ca-pv and Mg-pv will not mix in pyrolytic compositions in lower mantle except possibly in deep hot parts of the lower mantle.

Defect elements, such as Fe, Al, and Ti may, however, play important roles in the mixing of these phases. Creasy et al. (2020) recently found that a pyrolytic mixture with around 1–5% Fe in the bridgmanite formed two distinct perovskite phases, Mg-pv and Ca-pv, at lower mantle conditions (up to 75 GPa and 2300 K) when it was reduced (pure ferrous iron) but one single phase when half of the iron was oxidized to ferric iron. Armstrong et al. (2012) clearly pointed out that the addition of titanium will enlarge the single-phase domain of $MgSiO_3$-$CaSiO_3$. Using ab-initio calculations we previously established (Muir et al. 2021) a simple conceptual model to explore the influence of different impurities on the miscibility of Ca-pv and Mg-pv and found that large amounts of any defect element (>~1%) were required to significantly affect miscibility. This model had numerous omissions, however, and needs to be extended for any relevant element. Iron is the most prominent defect element in pyrolytic compositions and thus is a key candidate for potentially changing the dynamics of this phase mixing. In the lower mantle, iron concentration in bridgmanite is around ~10% (Irifune et al. 2010), and it may be even higher near the Core Mantle Boundary (CMB). Fujino et al. (2004) explored the effect of iron on the perovskite two-phase mixing using laser heated DAC and TEM. They found that the solid solubility of Mg in davemaoite was 4% at ~30 GPa and 1930 K but increased to ~18% at 30 GPa and 1800 K when around 9% iron was added, which shows clearly that iron promotes miscibility at least to some degree. In Creasy et al.(2020) samples with 27% davemaoite and around 3% ferrous iron in the bridgmanite were not mixed up to 75 GPa and 2300 K, which suggests that the solubility is below this point. In both studies there are not enough *P*, *T*, and Fe% points to explore systematically the effect of iron on the miscibility of the two perovskites. In this study, we conduct theoretical calculations to examine the effect of iron concentration, pressure (*P*) and temperature (*T*) on the mutual solubility of Ca-pv and Mg-pv at the lower mantle conditions.

Specifically, we examine how varying the Ca and the Fe content of bridgmanite and davemaoite mixtures affects their solubilities. We shall thus define two terms Ca%, which is Ca/(Mg+Ca+Fe) × 100%, and Fe%, which is Fe/(Mg+Ca+Fe) × 100%. The calcium content varies in different compositions that can occur in the lower mantle. The Ca% of mid-ocean ridge basalt (MORB) is between 30–60% (Hirose 2002; Hirose et al. 2005; Ricolleau et al. 2010), of harzburgitic compositions about 1–3% (Michael and Bonatti 1985; Ringwood 1991), and of pyrolytic compositions around 7–13% (Kesson et al. 1998; Mattern et al. 2005; Ringwood 1991). Iron in the lower mantle can have multiple oxidation states (primarily +2 and +3) and structural sites (A and B) (Gialampouki et al. 2018; Muir and Brodholt 2020; Wang et al. 2019). To determine the effect of iron on A site mixing of Ca and Mg, we shall focus on ferrous iron at the A site. This is likely also the predominant oxidation state of iron across the lower mantle in the absence of aluminum (Wang et al. 2019). The iron content of bridgmanite in the lower mantle is about 10% (Irifune et al. 2010) but maybe lower or higher in some regions and so we shall study iron concentrations of 0–25%. While the iron concentration of bridgmanite may be low in the presence of ferropericlase the formation of a mixed perovskite phase may increase the favorability and thus the concentration of iron in perovskite structures and this favorability needs to be examined. Ferrous iron in bridgmanite is in a state of high spin (Shim et al. 2017; Shukla et al. 2015; Xu et al. 2015) under mantle pressures and temperatures and so all of our calculations will have iron fixed to the high-spin state.

Methodology

Computational details

The simulations were carried out by VASP (Kresse and Furthmüller 1996a, 1996b) using the projector-augmented-wave (PAW) method (Kresse and Joubert 1999) and the PBE formulation of GGA (Perdew et al. 1996, 1997). In all calculations, the following PAW potentials were used: Core region cutoffs are 2.3 atomic units (a.u.) for calcium (core configuration $1s^22s^22p^6$, $3s^23p^64s^2$ as valence), 1.9 a.u. for silicon (core configuration$1s^22s^22p^6$, $3s^23p^2$ as valence), 1.52 a.u. for oxygen (core configuration $1s^2$, $2s^22p^4$ as valence), 2.0 a.u. for magnesium (core configuration $1s^22s^2$, $2p^63s^2$ as valence), and 2.3 a.u. for iron (core configuration $1s^22s^22p^63s^23p^6$, $3d^74s^1$ as valence). Traditional DFT does not deal well with heavily correlated electrons such as the d electrons of Fe, and so some kind of correction is needed to capture their electron energy levels accurately. For this, the Hubbard U approach and the rotationally invariant formulation of GGA+U introduced by Dudarev et al. (1998) was used, where an additional localized energy penalty is introduced for intra-atomic interactions, in this case for 3d electrons in Fe. The empirical value of U_{eff} (U-J) was set to be 2.5 eV.

A unit cell of 40 atoms was used in static calculations (except for 6.25% Fe where 80 atom unit cells were used) and one with 80 atoms (2 × 2 × 1) in molecular dynamics (MD) simulations. In our calculations, $Mg_{1-x}Fe_xSiO_3$ and $Mg_{1-x-y}Fe_xCa_ySiO_3$ were modeled with an orthorhombic (*Pbnm*) unit cell. We also calculated *I*4/*mcm*, and *Pm*3*m* structures for $Mg_{1-x-y}Fe_xCa_ySiO_3$ but they were found to be less stable than a *Pbnm* structure at all *P* and *T* conditions. For $CaSiO_3$ both *I*4/*mcm* and *Pm*3*m* structures were modeled with *Pm*3*m* favored at high temperatures. Calculations were done at 25, 75, and 125 GPa (all pressures are uncorrected) and at 0 (static), 1000, 2000, and 3000 K (molecular dynamics). Static simulations (~0 K) were calculated with a (3 × 5 × 5) k-point mesh (4 × 4 × 4 for 6.25 Fe% iron), and molecular dynamics runs were conducted at the gamma point only. Both static and MD calculations had an energy cutoff of 500 eV and converged to within 10^{-5} eV. Molecular dynamics were performed in an NVT ensemble with the Nosé thermostat and fluctuations around 20 THz and energies were determined from a run of 2.5 ps.

Mixing thermodynamics

To find the solubility of $CaSiO_3$ in (Mg, Fe)SiO_3, we examined the following reaction:

$$x CaSiO_3 + (1 - x)\, Mg_{1-y}Fe_ySiO_3 \rightarrow Ca_xFe_{y(1-x)}Mg_{1-x-y+xy}SiO_3. \quad (1)$$

The iron is placed in Mg-pv before mixing is simulated. Although some iron must thermodynamically enter into Ca-pv as discussed in the text this amount is generally negligible and can be ignored. To determine mixing we calculate the free energy of reaction 1 using:

$$G_{mix} = H_{mix} - TS_{mix} \quad (2)$$

where $G_{mix} = 0$ represents the mixing boundary, and mixing occurs when G_{mix} of Equation 1 is negative. T_{mix} is the mixing tempersature defined as the *T*, which makes $G_{mix} = 0$ (i.e., the solvus temperature). H_{mix} is the mixing enthalpy. Determining S_{mix} (the mixing entropy) is complex; in our case we have defined it as the sum of configurational and vibrational entropies.

For the configurational entropy, for each specific calcium and iron content in the unit cell we calculated the relative enthalpy of different configurations of Fe, Ca, and Mg, where a configuration is the arrangement of Fe, Ca, and Mg across the A lattice sites. We then used this equation (Gibb's entropy equation) to calculate S_{Config}:

$$S_{Config} = -k_B \sum_i \frac{1}{\sum_i e^{\frac{-E_i}{k_B T}}} e^{\frac{-E_i}{k_B T}} \ln \frac{1}{\sum_i e^{\frac{-E_i}{k_B T}}} e^{\frac{-E_i}{k_B T}} \quad (3)$$

where k_B is Boltzmann constant, T is temperature and E_i is the relative energy of each configuration. Strictly speaking S_{Config} should be determined with the relative energy of each configuration including their high-temperature components. Practically the difference in phonons between different configurations should be small particularly if their relative enthalpy is small, which is indicative of no large structural rearrangements. As outlined in the text, we find enthalpy differences between different arrangements to not be large. Thus, we shall use the relative enthalpy in each case when calculating using Equation 3. The number of theoretical arrangements in each case is

$$Z = \frac{N!}{N_{Mg}!* N_{Ca}!* N_{Fe}!}$$

(N is the sum of Mg, Ca, and Fe).

To calculate configurational entropy, we calculated the relative enthalpy of all possible arrangements of Fe, Ca, and Mg in our 40 atom unit cells when these atoms were confined to relaxed A lattice sites. This was done with Ca% = 0, 12.5, 25, 37.5, 50, 62.5, 75, and 100 and with 0, 1, or 2 irons (Fe% = 0, 12.5, and 25%) at 25, 75, and 125 GPa with the solutions to Equation 2 given in Online Materials[1] Table S1. In addition, we calculated the "perfect" entropy, which is the entropy if all arrangements had the same energy, the Boltzmann entropy. This is done via $S_{Config} = k_B \ln Z$ where Z is the total number of arrangements of all atoms as outlined above. We found that the difference between the two calculation methods is very small. Therefore, our configuration entropy for mixing in this study was calculated by the formula $S_{Config} = k_B \ln Z$ and the more detailed results in Online Materials[1] Table S1 were ignored.

For vibrational entropy (S_{vib}), we obtain the velocity autocorrelation function through molecular dynamics calculations. The vibrational entropy is then determined by:

$$S(v) = \frac{2}{k_B T} \sum_{i=1}^{N} \sum_{k=1}^{3} m_a s_a^k \tag{4}$$

$$S_{vib} = k_B \int_0^\infty S(v) dV \tag{5}$$

where N is the number of atoms in the system, m_a is the mass of atom a, s_a^k is the spectral density of atom a in the direction k (x = 1, y = 2, z = 3), and V is the velocity. Errors were assessed using the Flyvbjerg technique (Flyvbjerg and Petersen 1989) and were <1.5 meV/atom in all cases. We propagated these errors as will be seen in a later figure and find that due to the similar energy of the mixed and unmixed phase, even this small error can add ± ~100 K to the mixing temperature.

To determine partitioning between two phases, we first determined G of each phase as a function of iron content. This was done by plotting the variation in H_{mix} and S_{vib} with our calculated points and fitting polynomials and through the analytical form of S_{Config}. For a fixed amount of iron, we then partitioned iron between the two phases until G was minimized.

In summary, for any condition (Ca%, Fe%, P) the mixing temperature is determined as such. We first calculated the enthalpy of mixing at a set pressure. For 0% iron content, this was done in 40 atom unit cells at 0, 12.5, 25, 37.5, 50, 62.5, 75, 82.5, and 100 Ca% content. For 6.25% iron content this was done in 80 atom unit cells at 0, 12.5, 25, 50, and 100 Ca% content. For 12.5% iron content this was done in 40 atom unit cells at 0, 6.25%, 12.5%, 25%, 50%, 75%, and 100% Ca% content. For 25% iron content this was done in 40 atom unit cells at 0, 6.25%, 12.5%, 25%, 62.5%, and 100% Ca% content. Before mixing iron was partitioned into its favored phase, Mg-pv (see text), we extrapolated the mixing enthalpies using second-order polynomials across first Ca%, then Fe% and then pressure to determine enthalpies at points beyond this. The configurational entropy of mixing was then determined at a set composition using the Boltzmann entropy (which is insensitive to pressure) at the required temperature. Vibrational entropy was added using the results of iron free systems as outlined in our recent study (Muir et al. 2021) with the contribution of iron to vibrational entropy ignored as explained earlier. Configurational and vibrational entropy was added to the mixing enthalpies and the temperature varied until Equation 1 equals 0.

Results and Discussion

Fe partitioning

The partitioning of ferrous iron (K_D) between different possible phases (Ca-pv, Mg-pv, and the mixed phase) will be a strong control on perovskite phase mixing and thus must be first considered. If ferrous iron is strongly favored in the mixed phase this will increase the favorability of phase mixing and vice versa. The strength of partitioning will also determine some of the dynamics of phase mixing. For example, a strong preference for ferrous iron to enter the mixed phase would lead to a wide phase loop, whereas a weak favorability would lead to a narrow phase loop. A strong preference for ferrous iron to enter the mixed phase could also lead to a mechanism by which iron-rich regions of the mantle could phase mix and become dynamically separated from the rest of the mantle.

In the lower mantle a third phase is present, that of ferropericlase. In a pure Ca-free bridgmanite ferrous iron prefers ferropericlase over bridgmanite (Muir and Brodholt 2016). On the surface the presence of Ca should not change this preference and thus it could be considered that bridgmanite in the lower mantle is iron-free and that we could ignore the effect of iron on mixing altogether. This story will change, however, if the presence of Ca enables the formation of a mixed phase into which ferrous iron prefers to partition over both bridgmanite and ferropericlase and thus we shall examine whether this is likely to be the case. Such an effect could change distribution of iron across the lower mantle as a whole. A likely pathway for this effect would be (A) iron-rich bridgmanite + iron-poor ferropericlase → iron-poor bridgmanite + iron-rich ferropericlase → iron-poor mixed phase + iron-rich ferropericlase → iron-rich mixed phase + poor iron ferropericlase. Pathway B would be iron-rich bridgmanite → iron-rich mixed phase, which is thermodynamically identical to pathway A if they both run to completion and thus shall be calculated here though pathway A is more likely in a real mantle.

We consider two Fe partitioning coefficients, one between $MgSiO_3$ and $CaSiO_3$ ($K_{D1}^{Fe} = X_{Fe}^{Mg-pv}/X_{Fe}^{Ca-pv}$) and one between $MgSiO_3$ and $(Mg_{1-x}Ca_x)SiO_3$ [$K_{D2}^{Fe} = X_{Fe}^{Mg-pv}/X_{Fe}^{(Mg_{1-x}Ca_x)SiO_3}$]. In both cases we only consider ferrous iron and a value above 1 means iron prefers bridgmanite over the alternative. Some values for these are given in Table 1 and Figure 1. K_{D1} considers a case where Ca-pv partitions iron out of bridgmanite and that interferes with Pathway A or B. We find that K_{D1} is always >1 and that Fe^{2+} always prefers to partition into Mg-pv over Ca-pv. Thus Ca-pv can be considered as an iron-free phase and in a Mg-pv and Ca-pv mixture all iron shall be considered partitioned into Mg-pv as in reaction 1. For a few systems we tested the effect of including K_{D1} partitioning and allowed iron to partition into both davemaoite and bridgmanite before forming a perovskite mixed phase but we found no substantial changes (<20 K, generally below <5 K) to our values of T_{mix}. K_{D2} calculates partitioning of Fe^{2+} across pathway B. We find that except for very large amounts of Fe^{2+} at low pressures (where mixing is not expected to occur), Fe^{2+} always favors the mixed phase over Mg-pv (K_{D2} <1) and that this preference increases with pressure. The amount of Fe^{2+} in the system has an effect on the value of K_{D2} but this is small as shown in Figure 1. In no cases at high pressure (where mixing is likely to occur) does Fe^{2+} favor bridgmanite over the mixed phase. This preference is not particularly strong, however, with all K_{D2} values being above 0.25 excepts in cases with extreme iron contents or in a basaltic mixture.

As discussed above Fe^{2+} could potentially partition from bridgmanite either to ferropericlase or to the mixed phase. We can examine this by comparing our K_{D2} values for Fe^{2+} going

Table 1. The partitioning coefficient of Fe between $MgSiO_3$ and $CaSiO_3$ ($K_{D1}^{Fe} = X_{Fe}^{Mg\text{-}pv}/X_{Fe}^{Ca\text{-}pv}$) and between $Mg_{1-x}Ca_xSiO_3$ (x = 0.125/0.5) and $MgSiO_3$ [$K_{D2}^{Fe} = X_{Fe}^{Mg\text{-}pv}/X_{Fe}^{(Mg_{1-x}Ca_x)SiO_3}$] at 25–125 GPa and 1000–3000 K

	K_{D1}		
	1000 K	2000 K	3000 K
25 GPa	3.116	1.765	1.461
75 GPa	6.548	2.559	1.871
125 GPa	21.815	4.671	2.794

	K_{D2}(x = 0.125)					
	2000 K		2500 K		3000 K	
	6.25%Fe	25%Fe	6.25%Fe	25%Fe	6.25%Fe	25%Fe
25 GPa	0.634	4.485	0.694	3.322	0.738	2.719
75 GPa	0.446	0.809	0.524	0.844	0.583	0.868
125 GPa	0.372	0.882	0.434	0.759	0.471	0.633

	K_{D2}(x = 0.5)					
	2000 K		2500 K		3000 K	
	6.25%Fe	25%Fe	6.25%Fe	25%Fe	6.25%Fe	25%Fe
25 GPa	0.407	0.227	0.487	0.305	0.549	0.372
75 GPa	0.190	0.006	0.264	0.016	0.330	0.031
125 GPa	0.070	0.002	0.114	0.005	0.155	0.010

from bridgmanite to the mixed phase to calculated K_D values of Fe^{2+} going from bridgmanite to ferropericlase. Muir and Brodholt (2016) claimed that there is a strong partitioning of ferrous iron from bridgmanite to ferropericlase with a K_D of ~0.32 at 30 GPa dropping to ~0.06 at 120 GPa at 2000 K and dropping further with increased temperature. This is a much stronger preference for ferrous iron going into ferropericlase than into the mixed phase and so the preference of ferrous iron at deep mantle pressures and temperatures where mixing occurs is ferropericlase > the mixed phase > bridgmanite in that order. Thus, the formation of a perovskite mixed phase does not outcompete ferropericlase as an iron sink and should not substantially alter the distribution of iron in the deep lower mantle. Phase mixing is thus not a way to produce iron-rich regions in the lower mantle. Our concentrations of iron in the rest of this paper shall refer to the concentration of ferrous iron in the perovskite phases (bridgmanite and the mixed phase). In a real lower mantle with ferropericlase this concentration will be lower than the concentration of iron in the system and could be up to 20 times lower as you approach the CMB (Muir and Brodholt 2016).

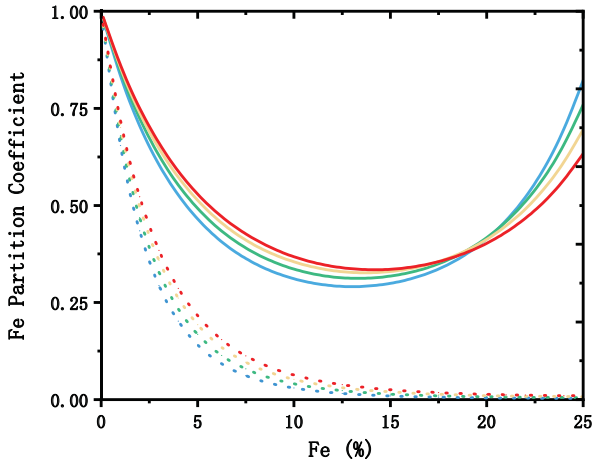

Figure 1. Plot of the partitioning coefficient of Fe ($K_{D2}^{Fe} = X_{Fe}^{Mg\text{-}pv}$ / $X_{Fe}^{(Mg_{1-x}Ca_x)SiO_3}$) between $Mg_{1-x}Ca_xSiO_3$ with x = 0.125 (solid line) / 0.5 (dashed line) and $MgSiO_3$ at 125 GPa and 2250–3000 K. Blue line represents 2250 K; green, 2500 K; yellow, 2750 K; and red, 3000 K. This was determined by first calculating G of each phase as a function of the partitioning at Fe% = 0, 6.25, 12.5, and 25%. (Color online.)

Effect of iron on mixing energies

In this section we shall examine the effect of ferrous iron on the individual energetic components of mixing.

H_{mix}. We determined the effect of ferrous iron on the mixing enthalpy (ΔH_{mix}) using static DFT calculations with the results shown in Figure 2 (and more data are presented in Online Materials[1] Table S2). H_{mix} is always positive, which shows that Ca-pv and Mg-pv are naturally immiscible and that temperature is required to mix them. With increasing pressure H_{mix} increases, which will lead to a decrease in the favorability of mixing. Fe^{2+} in general decreases H_{mix} and thus promotes phase mixing, but this trend is nonlinear with iron concentration. Initially H_{mix} decreases with an increasing iron concentration but after a specific iron concentration is reached H_{mix} then increases with increasing iron concentration. The reason for this nonlinearity can be seen in Online Materials[1] Figure S1, which plots the change in energy of $Mg_{1-x}Fe_xSiO_3$ and $Mg_{1-x-y}Fe_xCa_ySiO_3$ as a function of Fe^{2+} concentration. Replacing Mg with Fe has a similar effect on the enthalpies of the mixed phase and Mg-pv as both structures are extremely similar. Hence, the effect of iron on the enthalpy difference between these two systems is highly sensitive to small structural relaxations, and thus deviations from linearity are seen. Such deviations grow larger as the iron concentration increases and both mixed and unmixed structures begin to transition to an iron-rich end-member, which has significant structural and energetic differences to the Mg-rich end-member. While the effect of substitutional defects on properties like enthalpy are generally linear with concentration, these defects are usually present in much smaller concentrations than are seen for Fe in bridgmanite. At high-defect concentrations (such as above ~10% Fe^{2+}) defect-defect interactions are significant and can cause nonlinear deviations to H_{mix} when the enthalpy difference between

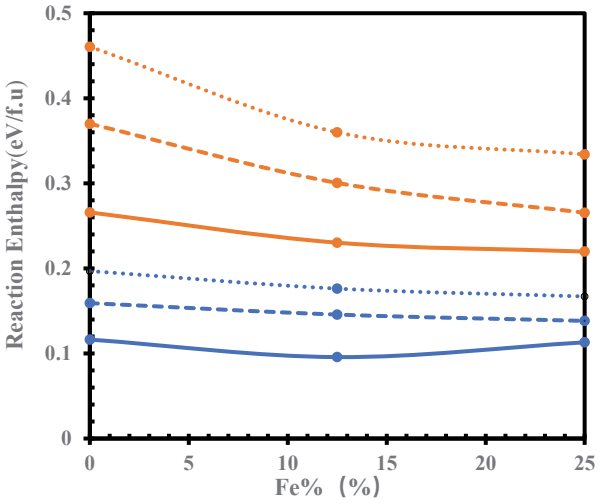

Figure 2. Reaction enthalpies (H_{mix}) of reaction 1 with x = 12.5% (blue line) and 50% (orange line), as the function of iron contents at three pressures of 25 GPa (solid line), 75 GPa (dashed line), and 125 GPa (dotted line), respectively. (Color online.)

the starting and ending products is small. It is important to stress that for structures considered in our reactions and for each Ca% and Fe% considered, we calculated the enthalpy of all possible configurations of Fe, Ca, and Mg in our models and used the lowest enthalpy. Thus, this nonlinear trend is not an artifact of the favored arrangement of iron in these systems changing with concentration. The relative enthalpy of different iron configurations with a fixed composition can vary by up to 0.15 eV/f.u. and so is similar to the energy difference between unmixed and mixed phases.

***S*Config.** We examined the effect of different iron arrangements, as explained in the methods, to estimate the effect of iron on configurational entropy (S_{config}) of end-members and mixed systems. In a perfect system (where all arrangements of atoms are energetically equivalent) the presence of iron does not cause an increase to S_{config} during mixing. This is because iron exists on the A site where mixing between Mg and Ca occurs in the perfect system and because iron is primarily partitioned to a single phase before mixing. As shown in Online Materials[1] Table S1, the configurational entropy of the both iron-bearing Mg-pv and the Fe,Mg,Ca-bearing mixed phase is near the perfect Boltzmann entropy limit. At all conditions, the difference between a perfect Boltzmann configurational entropy and our calculated configurational entropy is <~4 meV/atom. This is a very small energy term and is much smaller than the H_{mix} term. This suggests that all arrangements of Mg, Fe, and Ca on the A sites in both Mg-pv and the mixed phase are effectively equivalent and that iron does not cause large structural rearrangements in Mg-pv or the mixed phase. This means that the effect of iron on the configurational entropy of mixing can largely be approximated by considering it as an ideal system. In other words, iron does not cause an increase in mixing S_{Config} and does not promote mixing in this way. Considering a system with 12.5% Fe and 12.5% Ca, changing between perfect and non-perfect S_{Config} changes the mixing temperature by ~50 K. Thus, the primary effect on iron on mixing should be enthalpic and effect of iron on S_{Config} can largely be ignored. These results are a vindication of one of the assumptions in the model of Muir et al. (2021), where S_{Config} was treated using the perfect Boltzmann limits.

***S*vib.** Vibrational entropy (S_{vib}) depends on long-range phonons and is likely unaffected by the addition of defects in small concentrations but could be strongly affected by defects present in large quantities like Fe. S_{vib} is essential to calculating mixing parameters of these systems (Muir et al. 2021), but we predict that ΔS_{vib}-Fe (the change caused to S_{vib} by iron) is not essential. Iron makes no large structural rearrangements to the system as indicated by its near-perfect values of S_{Config} and thus likely also has small effects on long-range vibrational entropy. The change in the vibrational entropy term from replacing a Mg atom with an iron atom is calculated to be extremely small (Table 2), particularly at high pressures where mixing occurs. With the conditions in Table 2 including an ΔS_{vib}-Fe term changes T_{mix} at 25 GPa by <50 K but by <0.5 K at 125 GPa at conditions where mixing occurs. Therefore, in this work we shall include S_{vib} but ignore the effects of ΔS_{vib}-Fe. These results are a vindication of one of the assumptions in the model of Muir et al. (2021) where ΔS_{vib}-X was ignored when introducing defect elements.

Mixing. Previously the mixing of iron-free forsterite was explored and compared with experimental results in Muir et al. (2021). In that work it was found that a pyrolytic mixture of pure Mg-pv and Ca-pv will not mix along normal geotherms before the D″ layer.

TABLE 2. Value of ΔS_{vib}-Fe (the change in the vibrational entropy term from replacing a Mg atom with an Fe atom) for adding 1 iron to 80-atom bridgmanite (Fe% = 6.25) and the mixed phase with Ca% = 50

		ΔS_{vib}-Fe (meV/atom)	
Pressure (GPa)	Temperature (K)	Bridgmanite	Mixed phase
25	1000	−2.6	−0.3
	2000	−2.2	−0.1
	3000	−1.6	−0.3
125	1000	−4.1	−4.0
	2000	−4.0	−3.9
	3000	−3.8	−4.4

In this work we shall focus on how iron could change this picture.

In Figure 3, we plot the T_{mix} of a 1:7 (pyrolytic) mixture of davemaoite and Bridgmanite as a function of iron at pressures of 25, 75, and 125 GPa. When iron is initially added into the system, the mixing temperature decreases by about 80 K per 1% Fe. This T_{mix} decrease in a pyrolytic mixture does not continue universally with concentration, however, and a T_{mix} minimum is seen at ~13% Fe. Beyond this increasing the ferrous iron concentration causes T_{mix} to rise. Overall, this means that while a small amount of iron (6.25%) causes a T_{mix} decrease of 500 K a large amount of iron (25%) causes a much smaller decrease in T_{mix} (<100 K). As shown in Figure 2, the Fe induced decrease in H_{mix} is largest at ~13% and is smaller at either side of this.

Figure 3 also shows the effect of iron on a 1:1 mixture of Ca-pv and Mg-pv (Ca% = 50, basaltic). In this case, unlike the pyrolytic case, T_{mix} decreases with increasing iron concentration continually up until 25%. A likely explanation for the different behaviors between pyrolytic and basaltic compositions is due to iron partitioning preferences. The iron partitioning coefficient (K_{D1}^{Fe}) between $MgSiO_3$ and $CaSiO_3$ is generally large, with strong partitioning of Fe into the Mg end-member. The iron partition coefficient (K_{D2}^{Fe}) between bridgmanite and the mixed phase is smaller and closer to 1, particularly at lower pressures. Thus, there is a strong dislike of Fe going into Ca sites rather than Mg sites as Fe^{2+} is much closer in size to Mg^{2+} than it is to Ca^{2+} (~78/72/100 pm, respectively). At low-ferrous iron concentrations iron partitions into the mixed phase and thus reduces the mixing temperature. As iron concentration increases relative to Ca concentration, iron will partition into the Mg-end-member and not take part in the miscibility process. Thus, it will cost energy to put the surplus iron back into the mixture (T_{mix} increase). The iron concentration at which a T_{mix} decrease is converted into a T_{mix} increase (the T_{mix} minimum) depends upon the relative amount of Fe sites vs. Ca sites. When Ca% is 12.5% (pyrolytic mixture), the iron-driven two-phase solid solution T_{mix} minimum is around 13% Fe but when Ca% is 50% (basaltic mixture) this T_{mix} minimum increases to ~30% Fe.

Figure 4 presents the solubility of $CaSiO_3$ and $MgSiO_3$ with different amounts of iron at a deep lower mantle pressure (125 GPa). In low-iron, moderate-iron and iron-free systems solubility rises sharply with temperature when Ca% is low before reaching a plateau where solubility rises much slower with temperature. In high-iron system solubility has much more complex effects with Ca% due to the rising incompatibility of Fe and Ca as discussed above. Thus, at deep pressures T_{mix} is similar for a pyrolytic (Ca% = 12.5% 2518 K) and a basaltic (Ca% = 50% 2593 K) composition in the absence of iron. With the introduction of moderate amounts of iron 6.25%/12.5% iron this harmony is maintained

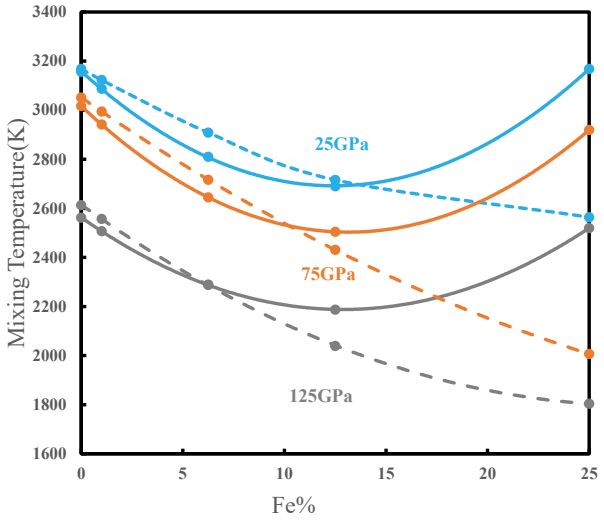

FIGURE 3. Plot of the mixing temperature (T_{mix}) for mixtures of Ca-pv and Mg-pv as a function of iron concentration. Solid lines have Ca: Mg = 1:7 (solid line) and dashed line 1:1. Blue lines represent 25 GPa, orange lines 75 GPa, and gray lines 125 GPa. (Color online.)

as T_{mix} reduces to ~2280 K/~2180 K for the pyrolytic mixture and ~2290 K/2040 K for the basaltic mixture, respectively. The introduction of a large amount of iron (25% Fe), however, causes T_{mix} to vary wildly between the pyrolytic (~2520 K) and basaltic (~1850 K) compositions.

The most direct experimental measurement of the effect of iron on T_{mix} comes from Fujino et al. (2004). Comparisons with that work are difficult, however, due to the high concentrations of Fe in their samples (with Fe nearly equivalent to Mg) and due to its focus on the Ca-pv side of the solubility diagram. As discussed above, the behavior of solubility in the presence of high-iron concentrations is not easy to predict and the concentrations of iron in Fujino et al. (2004) are beyond the scope of our calculations. Nevertheless, our study is consistent with the findings of Fujino et al. (2004) in that iron can promote the miscibility of two perovskite phases. A comparison can also be made with Creasy et al. (2020). In the presence of pure ferrous iron, mixing was not seen in a sample with 27% Ca that was placed under pressure from 35–75 GPa and heated up to 2300 K. At 75 GPa, we predict T_{mix} for this system to be 2942 K with 3% ferrous iron and 2850 K with 5% ferrous iron and thus we also predict that these phases should not mix.

The effect of ferrous iron concentration on T_{mix} is thus strongly nonlinear. This is very different from the simple model presented in Muir et al. (2021), which assumed a linear effect of ferrous iron concentration on T_{mix}. This nonlinearity is largely due to nonlinear variations in H_{mix} and stresses the importance of fully calculating the effect of defective elements rather than simple extrapolations. The model in Muir et al. (2021) is thus generally valid at low iron concentrations but overestimates the effect of Fe on T_{mix} at high iron concentrations. This leads to quite different implications as the simple linear model would state that high-iron systems are extremely likely to have perovskite phase mixing in the mantle and could segregate iron from the regular mantle but as we demonstrate here high-iron systems are actually less likely to have perovskite phase mixing than low-iron systems.

When considering other defect elements, the simple linear concentration model of Muir et al. (2021) is more likely to apply than it does to iron. There are two reasons. First, iron has very large concentrations in bridgmanite, whereas most defective elements have smaller concentrations. Nonlinear modifications to H_{mix} are more likely as the concentration of defects increases. Below ~10% ferrous iron, nonlinear modifications to H_{mix} are small, and the linear model of Muir et al. (2021) and the model presented here predict very similar T_{mix} values. Most defective elements in bridgmanite will have concentrations much lower than this and thus H_{mix} is expected to behave linearly with the concentration of the defect. The second reason is that Fe^{2+} and Mg^{2+} are very similar and thus replacing Mg^{2+} with Fe^{2+} causes very small structural distortions in both bridgmanite and the mixed phase. This leads to the effect of iron on H_{mix} to be small and thus varying the concentration of iron does not cause large effects on H_{mix}. As defective elements become more dissimilar to those found in bridgmanite they will induce larger structural distortions to bridgmanite and the mixed phase and thus will induce larger changes to H_{mix}, which will be much more linearly dependent on defect concentration. Thus, other defective elements are speculated to have much more linear effects on H_{mix} with varying defect concentration and to be much closer to the linear model found in Muir et al. (2021).

We shall now explore how iron could affect mixing of a pyrolite across the lower mantle. Figure 5 presents the T_{mix} of a pyrolytic mixture (Ca% = 12.5) as a function of depth and iron concentration. Regardless of the amount of iron no mixing is predicted at the top of the lower mantle. With the concentration of iron that causes the maximum favorability of mixing (~13%) perovskite phase mixing is predicted to occur at ~70 GPa in the hottest parts of the mantle. As the iron concentration increases or decreases or the mantle cools then mixing only occurs at deeper parts of the mantle. A ferrous iron concentration of 13% would be an extremely iron rich part of the mantle, especially when considering the effects of ferropericlase, and more reasonable perovskite iron concentrations lie between 0–6.25%. With these iron concentrations and the "standard" geotherm, mixing is predicted to occur between 115–125 GPa depend-

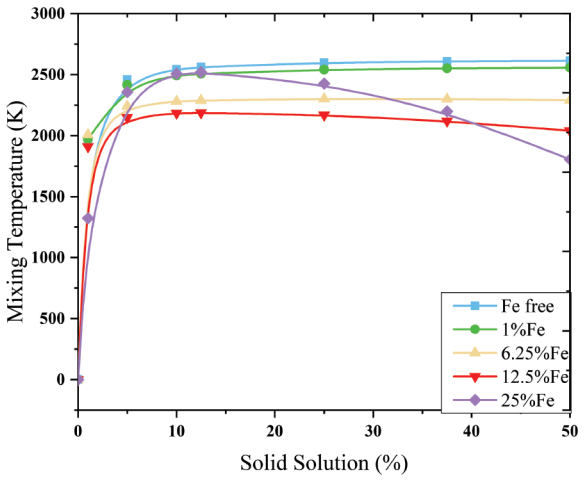

FIGURE 4. Solid solubility of Ca in bridgmanite as a function of mixing temperature at 125 GPa. The blue line represents the univariant Fe concentration with light blue, green, yellow, red, and purple representing 0, 1, 6.25, 12.5, and 25%, respectively. (Color online.)

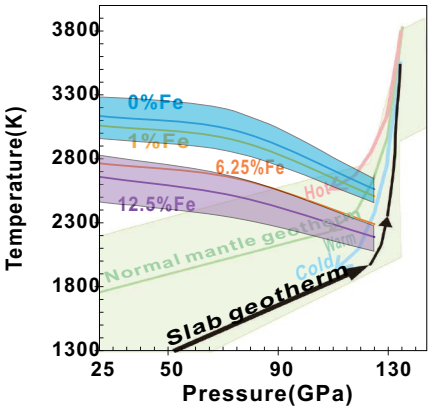

Figure 5. Plot of the mixing temperature (T_{mix}) for a mixture of Ca-pv and Mg-pv with Ca:Mg = 1:7 mixture and 0% Fe (blue line), 1% Fe (yellow line), 6.25% Fe (orange line), and 12.5% Fe (purple line). Various geothermal gradients alongside a cold subduction slab geothermal gradient are also presented for guidance (Ohtani et al. 2018). (Color online.)

ing upon the iron concentration. Thus, in a pyrolytic mantle ferrous iron causes only very small changes to the depth at which phase mixing is predicted to occur and the concentration of iron is not a large control on this process. Temperature fluctuations would be a much stronger control. Similar observations can be made with a basaltic composition (Online Materials[1] Fig. S2), but in this case the higher value of Ca% means no phase mixing is predicted to occur under any conditions.

Iron-rich regions present an interesting case. Various regions, particularly those near the CMB, have been speculated to be iron rich and these could present quite different behavior from the rest of the mantle. We find however that large amounts of iron decrease the stability of the mixed phase and do not promote its formation. Thus, these regions would not have different phase mixing characteristics from the rest of the iron-poor mantle. The potential formation of a mixed phase also does not provide a mechanism for forming iron-rich regions. A strong partitioning of iron from bridgmanite to the mixed phase could provide a physical mechanism for dynamically separating iron from the overall mantle across the physical barrier of a phase transition, but the partitioning coefficient of ferrous iron between bridgmanite and the mixing phase is small (Table 1) and moves closer to 1 with increasing iron (Fig. 1) and thus this mechanism is unlikely.

So far, we have considered only univariant mixing but the introduction of iron will lead to a phase loop. Calculating the exact dimensions of this phase loop is challenging. The similar trends of formation enthalpies vs. Fe% for Mg-pv and the mixed phase (Online Materials[1] Fig. S1) and their highly variable relationship to each other mean that constraining the phase loop requires very high accuracy in both the number of Fe concentrations that are measured and the precision of those points. This is potentially important future work but the phase loop is unlikely to be large or important simply due to K_{D2} being near 1. A wide phase loop would require strong partitioning of the iron to either Mg-pv or the mixed phase. Using a common tangent method, we calculate that at 125 GPa the width of the phase loop is <200 K at 6.25% Fe and <50 K at 12.5% Fe (both with Ca% = 12.5), but the method is not well constrained. Regardless it is difficult to propagate a wide phase loop in Fe space for the perovskite mixing reaction due to their close partitioning values and the phase loop must have widths of similar order to what are calculated here.

Finally, we consider the effect of other elements. The two other major components we expect to be important in perovskite phase mixing are ferric iron and aluminum. While ferrous iron is expected to be dominant over ferric iron (Xu et al. 2015) in deep lower mantle bridgmanite the presence of Al can convert ferrous iron to ferric iron by making Fe^{3+}-Al^{3+} and Al itself could affect mixing dynamics. The effect of these elements was studied with a simple linear enthalpic model in Muir et al. (2021) where it was concluded that Al raises the mixing temperature and Fe^{3+}-Al^{3+} causes the mixing temperature to remain largely static. While this was a simplistic model it correctly predict the trends seen for Fe^{2+} at low-Fe concentrations and thus model likely captures the broad trend of Ferric iron and aluminum in that they have little effect on mixing or slightly raise the mixing temperature. Thus, based on our model the presence of ferric iron and Al will likely not increase the favorability of phase mixing and our predictions above reflect conditions of maximum solubility. This effect is in contrast to Creasy et al.(2020) where an increase in ferric iron was predicted to increase mixing such that no mixing was seen with ferrous iron (as we also predict under their conditions) but mixing was seen with ferric iron. Determining the exact nature of these effects is complicated in that the oxidized sample in this work also had increased total iron (which increases mixing at these low temperatures) and a larger amount of Al in its sample (as higher ferric iron allows more Al to be adsorbed), which changes the dynamics significantly. It should be noted that these experiments lacked ferropericlase, which may partition out the iron in a real mantle. The presence of ferric iron (either in Fe-Fe or Al-Fe pairs) leads to an increase in S_{Config} upon mixing, so it would be expected to increase the favorability of perovskite phase mixing but in the model of Muir et al. (2021), this effect was opposed by penalties in H_{mix}. The results of Creasy et al. (2020), however, suggest that a simple linear model may not correctly reflect the effect of ferric iron and aluminum in perovskite phase mixing and a more detailed study of these species is required.

Implications

The effect of ferrous iron on the phase mixing of Ca-pv and Mg-pv was investigated. It is found that iron reduces the mixing temperature and increases miscibility but in highly nonlinear manners. Low-iron contents promote the mixing of these two phases but only to a small degree, whereas high iron contents have very little effect on the miscibility of these phases and can even hinder mixing. Ca-pv and Mg-pv should exist as independent phases in the lower mantle, but starting at 75 GPa in iron-rich hot mantle they can form a single phase. As iron content decreases or the mantle cools, the pressure of this transition deepens to around 120 GPa for a mantle at normal temperatures with a small amount of iron (~1% Fe in the perovskite). It is unclear what seismic signal would come about through such phase mixing. On phase mixing, there is a decrease in density, but this decrease is small (always <1% in our examined systems), which would likely prevent any large dynamical effects but the seismic properties of the mixed phase are unknown, so we cannot compare them to proposed lower mantle

heterogeneities such as LLSVPs though this would be useful work for the future. There is weak partitioning of iron from bridgmanite to the mixed phase, but this is less favorable than partitioning Fe from bridgmanite to MgO, and thus this is not expected to have strong dynamical consequences. Iron may not be a significant factor in determining the phases of the lower mantle as while moderate amounts of iron can drive significant mixing, it is more favorable for iron to exist in ferropericlase than the mixed phase, and there is no strong thermodynamic gradient to push iron into a mixed phase where it could be trapped in a dynamic mantle.

Funders

This work was supported by National Natural Science Foundation of China (41773057, 42050410319), with computational resources from Computer Simulation Labs of IGGCAS, the National Supercomputer Centers in Shenzhen and Beijing, China.

References cited

Anderson, O.L., Isaak, D.G., and Yamamoto, S. (1989) Anharmonicity and the equation of state for gold. Journal of Applied Physics, 65, 1534–1543, https://doi.org/10.1063/1.342969.

Armstrong, L.S., Walter, M.J., Tuff, J.R., Lord, O.T., Lennie, A.R., Kleppe, A.K., and Clark, S.M. (2012) Perovskite phase relations in the system CaO-MgO-TiO_2-SiO_2 and implications for deep mantle lithologies. Journal of Petrology, 53, 611–635, https://doi.org/10.1093/petrology/egr073.

Creasy, N., Girard, J., Eckert, J.O., and Lee, K.K.M. (2020) The role of redox on bridgmanite crystal chemistry and calcium speciation in the lower mantle. Journal of Geophysical Research: Solid Earth, 125, e2020JB020783, https://doi.org/10.1029/2020JB020783.

Dudarev, S.L., Botton, G.A., Savrasov, S.Y., Humphreys, C.J., and Sutton, A.P. (1998) Electron-energy-loss spectra and the structural stability of nickel oxide: An LSDA+U study. Physical Review B: Condensed Matter, 57, 1505–1509, https://doi.org/10.1103/PhysRevB.57.1505.

Flyvbjerg, H. and Petersen, H.G. (1989) Error-estimates on averages of correlated data. The Journal of Chemical Physics, 91, 461–466, https://doi.org/10.1063/1.457480.

Fujino, K., Sasaki, Y., Komori, T., Ogawa, H., Miyajima, N., Sata, N., and Yagi, T. (2004) Approach to the mineralogy of the lower mantle by a combined method of a laser-heated diamond anvil cell experiment and analytical electron microscopy. Physics of the Earth and Planetary Interiors, 143–144, 215–221, https://doi.org/10.1016/j.pepi.2003.11.013.

Gialampouki, M.A., Xu, S., and Morgan, D. (2018) Iron valence and partitioning between post-perovskite and ferropericlase in the Earth's lowermost mantle. Physics of the Earth and Planetary Interiors, 282, 110–116, https://doi.org/10.1016/j.pepi.2018.06.005.

Hirose, K. (2002) Phase transitions in pyrolitic mantle around 670-km depth: Implications for upwelling of plumes from the lower mantle. Journal of Geophysical Research: Solid Earth, 107, ECV 3-1–ECV 3-13, https://doi.org/10.1029/2001JB000597.

Hirose, K., Takafuji, N., Sata, N., and Ohishi, Y. (2005) Phase transition and density of subducted MORB crust in the lower mantle. Earth and Planetary Science Letters, 237, 239–251, https://doi.org/10.1016/j.epsl.2005.06.035.

Irifune, T., Susaki, J., Yagi, T., and Sawamoto, H. (1989) Phase-transformations in diopside $CaMgSi_2O_6$ at pressures up to 25-GPa. Geophysical Research Letters, 16, 187–190, https://doi.org/10.1029/GL016i002p00187.

Irifune, T., Miyashita, M., Inoue, T., Ando, J., Funakoshi, K., and Utsumi, W. (2000) High-pressure phase transformation in $CaMgSi_2O_6$and implications for origin of ultra-deep diamond inclusions. Geophysical Research Letters, 27, 3541–3544, https://doi.org/10.1029/2000GL012105.

Irifune, T., Shinmei, T., McCammon, C.A., Miyajima, N., Rubie, D.C., and Frost, D.J. (2010) Iron partitioning and density changes of pyrolite in Earth's lower mantle. Science, 327, 193–195, https://doi.org/10.1126/science.1181443.

Jung, D.Y. and Schmidt, M.W. (2011) Solid solution behaviour of $CaSiO_3$ and $MgSiO_3$ perovskites. Physics and Chemistry of Minerals, 38, 311–319, https://doi.org/10.1007/s00269-010-0405-0.

Kesson, S.E., Fitz Gerald, J.D., Shelley, J.M.G., and Withers, R.L. (1995) Phase-relations, structure and crystal-chemistry of some aluminous silicate perovskites. Earth and Planetary Science Letters, 134, 187–201, https://doi.org/10.1016/0012-821X(95)00112-P.

Kesson, S.E., Fitz Gerald, J.D., and Shelley, J.M. (1998) Mineralogy and dynamics of a pyrolite lower mantle. Nature, 393, 252–255, https://doi.org/10.1038/30466.

Kresse, G. and Furthmüller, J. (1996a) Efficiency of ab-initio total energy calculations for metals and semiconductors using a plane-wave basis set. Computational Materials Science, 6, 15–50, https://doi.org/10.1016/0927-0256(96)00008-0.

——— (1996b) Efficient iterative schemes for ab initio total-energy calculations using a plane-wave basis set. Physical Review B: Condensed Matter, 54, 11169–11186, https://doi.org/10.1103/PhysRevB.54.11169.

Kresse, G. and Joubert, D. (1999) From ultrasoft pseudopotentials to the projector augmented-wave method. Physical Review B: Condensed Matter, 59, 1758–1775, https://doi.org/10.1103/PhysRevB.59.1758.

Mattern, E., Matas, J., Ricard, Y., and Bass, J. (2005) Lower mantle composition and temperature from mineral physics and thermodynamic modelling. Geophysical Journal International, 160, 973–990, https://doi.org/10.1111/j.1365-246X.2004.02549.x.

Michael, P.J. and Bonatti, E. (1985) Peridotite composition from the North-Atlantic—regional and tectonic variations and implications for partial melting. Earth and Planetary Science Letters, 73, 91–104, https://doi.org/10.1016/0012-821X(85)90037-8.

Muir, J.M.R. and Brodholt, J.P. (2016) Ferrous iron partitioning in the lower mantle. Physics of the Earth and Planetary Interiors, 257, 12–17, https://doi.org/10.1016/j.pepi.2016.05.008.

——— (2020) Ferric iron in bridgmanite and implications for ULVZs. Physics of the Earth and Planetary Interiors, 306, 106505, https://doi.org/10.1016/j.pepi.2020.106505.

Muir, J.M.R., Thomson, A.R., and Zhang, F. (2021) The miscibility of calcium silicate perovskite and bridgmanite: A single phase perovskite in hot, iron-rich regions. Earth and Planetary Science Letters, 566, 116973, https://doi.org/10.1016/j.epsl.2021.116973.

Ohtani, E., Yuan, L., Ohira, I., Shatskiy, A., and Litasov, K. (2018) Fate of water transported into the deep mantle by slab subduction. Journal of Asian Earth Sciences, 167, 2–10, https://doi.org/10.1016/j.jseaes.2018.04.024.

O'Neill, B. and Jeanloz, R. (1990) Experimental petrology of the lower mantle—A natural peridotite taken to 54 GPa. Geophysical Research Letters, 17, 1477–1480, https://doi.org/10.1029/GL017i010p01477.

Perdew, J.P., Burke, K., and Ernzerhof, M. (1996) Generalized gradient approximation made simple. Physical Review Letters, 77, 3865–3868, https://doi.org/10.1103/PhysRevLett.77.3865.

——— (1997) Generalized gradient approximation made simple. Physical Review Letters, 78, 1396, https://doi.org/10.1103/PhysRevLett.78.1396.

Ricolleau, A., Perrillat, J.-P., Fiquet, G., Daniel, I., Matas, J., Addad, A., Menguy, N., Cardon, H., Mezouar, M., and Guignot, N. (2010) Phase relations and equation of state of a natural MORB: Implications for the density profile of subducted oceanic crust in the Earth's lower mantle. Journal of Geophysical Research, 115 (B8), B08202, https://doi.org/10.1029/2009JB006709.

Ringwood, A.E. (1991) Phase-transformations and their bearing on the constitution and dynamics of the mantle. Geochimica et Cosmochimica Acta, 55, 2083–2110, https://doi.org/10.1016/0016-7037(91)90090-R.

Shim, S.H., Grocholski, B., Ye, Y., Alp, E.E., Xu, S., Morgan, D., Meng, Y., and Prakapenka, V.B. (2017) Stability of ferrous-iron-rich bridgmanite under reducing midmantle conditions. Proceedings of the National Academy of Sciences, 114, 6468–6473, https://doi.org/10.1073/pnas.1614036114.

Shukla, G., Wu, Z.Q., Hsu, H., Floris, A., Cococcioni, M., and Wentzcovitch, R.M. (2015) Thermoelasticity of Fe^{2+}-bearing bridgmanite. Geophysical Research Letters, 42, 1741–1749, https://doi.org/10.1002/2014GL062888.

Tamai, H. and Yagi, T. (1989) High-pressure and high-temperature phase-relations in $CaSiO_3$ and $CaMgSi_2O_6$ and elasticity of perovskite-type $CaSiO_3$. Physics of the Earth and Planetary Interiors, 54, 370–377, https://doi.org/10.1016/0031-9201(89)90254-9.

Vitos, L., Magyari-Köpe, B., Ahuja, R., Kollár, J., Grimvall, G., and Johansson, B. (2006) Phase transformations between garnet and perovskite phases in the Earth's mantle: A theoretical study. Physics of the Earth and Planetary Interiors, 156, 108–116, https://doi.org/10.1016/j.pepi.2006.02.004.

Wang, X.L., Tsuchiya, T., and Zeng, Z. (2019) Effects of Fe and Al incorporations on the bridgmanite-postperovskite coexistence domain. Comptes Rendus Geoscience, 351, 141–146, https://doi.org/10.1016/j.crte.2018.10.003.

Xu, S., Shim, S.H., and Morgan, D. (2015) Origin of Fe^{3+} in Fe-containing, Al-free mantle silicate perovskite. Earth and Planetary Science Letters, 409, 319–328, https://doi.org/10.1016/j.epsl.2014.11.006.

Manuscript received October 17, 2021
Manuscript accepted March 5, 2022
Accepted manuscript online March 16, 2022
Manuscript handled by Jianwei Wang

Endnote:

[1]Deposit item AM-23-38356, Online Materials. Deposit items are free to all readers and found on the MSA website, via the specific issue's Table of Contents (go to http://www.minsocam.org/MSA/AmMin/TOC/2023/Mar2023_data/Mar2023_data.html).